Scripta Materialia 187 (2020) 434–438

Contents lists available at ScienceDirect

Scripta Materialia

journal homepage: www.elsevier.com/locate/scriptamat

Thermomechanical response of an ultrafine-grained nickel-yttrium alloy

S. Srinivasan[a], C. Kale[a], B.C. Hornbuckle[b], K.A. Darling[b], P. Peralta[a], K.N. Solanki[a,*]

[a] School for Engineering of Matter, Transport, and Energy, Arizona State University, Tempe, AZ 85287, USA
[b] Weapons and Materials Research Directorate, Aberdeen Proving Ground, MD 21005, USA

ARTICLE INFO

Article history:
Received 27 May 2020
Revised 14 June 2020
Accepted 20 June 2020
Available online 6 July 2020

Keywords:
Ultrafine-grained
Creep
Thermo-mechanical behavior
Grain growth

ABSTRACT

Thermomechanical behavior of an ultrafine-grained nickel-yttrium alloy has been investigated through quasi-static (10^{-4} s^{-1}) and high temperature creep experiments under uniaxial compression along with post-deformed transmission electron microscopy (TEM) characterization. While the alloy possesses a quasi-static flow stress of ~1255 MPa at room temperature, the flow stress drops by about 80% at 873 K. TEM analysis showed negligible average grain growth over the entire temperature range tested. Furthermore, the alloy showed exceptional steady–state creep behavior owing to the relative stability of the grain size and interactions between dislocations/grain boundary and inclusions/dispersoids.

Precipitate-strengthened polycrystalline alloys have been extensively studied and used since the discovery of the age hardening phenomenon almost a century back by Guinier [1]. In such class of materials, introduction of dispersoids has been critical in the development of advanced structural materials and provides a significant basis for designing new materials. In particular, the role of dispersoids as a core strategy in enhancing multitude of mutually exclusive properties (e.g. strength versus ductility) in a material has been extensively discussed lately [2–8]. For instance, the recent discovery of a nanocrystalline (NC) copper-tantalum alloy with nano-dispersoids has demonstrated a new paradigm in metallic alloy design, revealing extreme temperature and strain rate properties, as well as enhanced thermal and electrical conductivities [2,5,6,9–11]. A similar strategy was employed to develop a NC Fe-5at.%Zr alloy, which was shown to have enhanced creep resistance at 923 K due to numerous coherent and incoherent nano-precipitates that form in the grain interiors as well as along the grain boundaries [7]. At slightly larger grain sizes (400–500 nm), nanostructured ferritic steel (NFA) alloys that are a sub-class of oxide dispersion strengthened (ODS) alloys exhibit enhanced high temperature properties as well as radiation tolerance attributed to the dispersoids, making them potential candidate materials for widespread use in the nuclear industry [12–14]. Despite the rapid expansion of such findings, there still exists an important area for further development of new materials, particularly for sustainable transportation industries [15,16].

Nickel (Ni) and Ni based superalloys such as IN718 are widely used in transportation and power generation industries; however, the complexity in manufacturing process and cost limits their operating efficiency and ranges [16]. Reducing their grain size to NC and UFG regime can significantly improve mechanical properties, such as yield strength; however, the microstructural instability and grain boundary mediated deformation could be detrimental for high temperature applications [17–19]. Nonetheless, Darling et al. [20] have recently developed an ultrafine-grained (UFG) nickel-yttrium (Ni-Y) alloy that has been shown to be microstructurally stable during annealing up to 1373 K (0.8 T_m). Similarly, nanoindentation creep study of NC Ni-W indicated low temperature improvement in microstructural stability and creep properties due to alloying of W as compared to NC Ni [21]. In this work, the thermomechanical stability and high temperature properties of an UFG Ni-Y alloy are probed through quasi-static (10^{-4} s^{-1}) and high temperature creep tests under uniaxial compression, followed by transmission electron microscopy (TEM) analysis to understand the underlying mechanisms.

The Ni-Y alloy was synthesized with the desired UFG microstructure using powder processing techniques and controlling parameters such as milling temperature, milling time, equal channel angular extrusion (ECAE) temperature, and thermomechanical processing conditions as outlined in [20]. Elemental Ni and Y powders (−325 mesh and 99.9% purity), with appropriate weights to obtain the target Ni-5at.%Y composition, were loaded into a hardened steel vial along with the milling media (440C stainless steel

* Corresponding author.
E-mail address: kiran.solanki@asu.edu (K.N. Solanki).

https://doi.org/10.1016/j.scriptamat.2020.06.068
1359-6462/

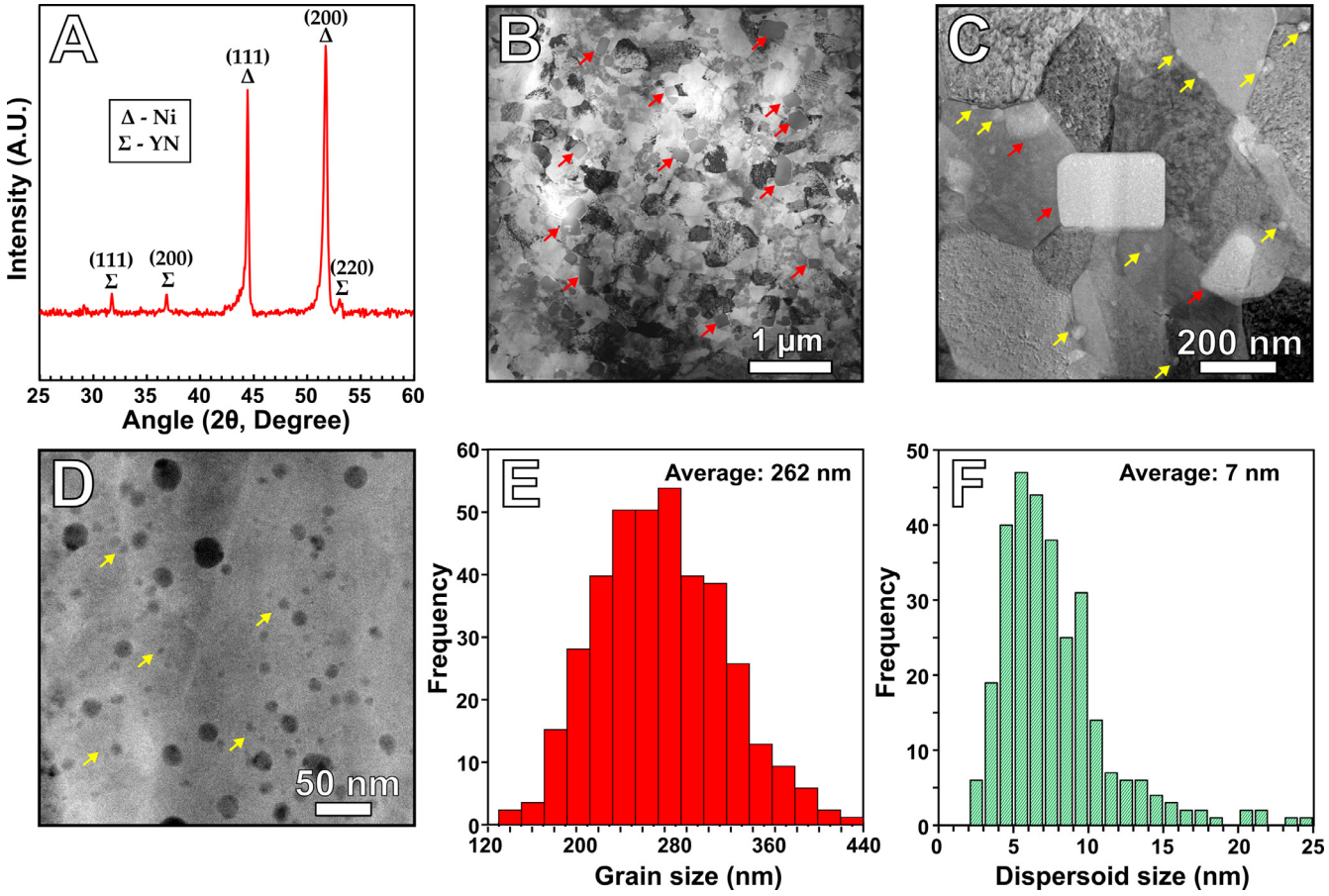

Fig. 1. (A) XRD spectrum of as-received Ni-Y alloy showing presence of Ni and YN phases. (B) Low mag Bright field (BF) STEM image of as-received Ni-Y alloy highlighting cuboidal YN phases with red arrows. (C) Medium mag BF STEM image highlighting cuboidal YN phases with red arrows and yttrium nanodispersoids along the grain boundaries with yellow arrows. (D) High mag HAADF image highlighting yttrium nanodispersoids with yellow arrows. (F) Number distribution of dispersoid size for Ni-Y alloy in the as-received condition. (For interpretation of the references to color in this figure legend, the reader is referred to the web version of this article.)

balls) inside a glove box with an Ar atmosphere (oxygen and H_2O are $<$ 1 ppm). The ball to powder ratio was maintained at 10:1. A SPEX 8000M shaker mill was utilized to perform the milling at cryogenic temperature (verified to be ~ −196 °C) for 8 h using liquid nitrogen. The Ni- 5at.% Y powder was consolidated to bulk via equal channel angular extrusion (ECAE). Before starting the ECAE process, the die assembly used for processing the billets was preheated to 623 K (350 °C) to minimize thermal loss during the ECAE processing. The billets, heated and equilibrated to 1373 K (1100 °C) for 40 min, were dropped into the ECAE tooling as quickly as possible from the furnace and extruded at a rate of 25.5 mm/s. These steps were repeated 4 times following route Bc to prevent imparting a texture to the consolidated powder [22]. By extruding through an angle of 90°, a total strain of 460% was imparted onto the powder-containing billet because of processing.

Cylindrical specimens (3 mm in length and 3 mm in diameter) for mechanical testing were then machined from these billets, within the region containing the consolidated powder, via wire electric discharge machining. Uniaxial compression tests were carried out at a strain rate of 10^{-4} s^{-1} at various temperatures, on an INSTRON load frame equipped with a 50 kN load cell and a high temperature clam-shell furnace. Compression creep testing was done under constant load (in lab air) on an ATS Series 2320-MM Lever Arm Tester. As-received (after ECAE processing) as well as post-deformed microstructure were analyzed using TEM, and X-ray diffraction (XRD) was utilized for phase identification. Specimens for TEM were prepared using the conventional thinning and dimpling of 3 mm disks to 70 μm and 5 μm thickness respectively, followed by ion milling using a Gatan Precision Ion Polishing System (PIPS) at liquid nitrogen temperatures to obtain electron-transparent regions in the center. The specimens were then plasma cleaned in Ar to reduce contamination prior to TEM observations on an aberration corrected JEOL ARM-200F operated at 200 keV.

Fig. 1 shows results from microstructural characterization of as-received Ni-5at.%Y. XRD characterization (Fig. 1A) identified the presence of Ni and YN phases. Exposure of the milled elemental powders to small amounts of nitrogen (N_2) during cryogenic milling resulted in the formation of yttrium nitride phase. Further details related to the processing and impurity levels can be found in [20]. The TEM micrographs, shown in Fig. 1B and C indicates an UFG microstructure with two phases. Energy dispersive x-ray spectroscopy (EDS) analysis (Fig. S1B and D) showed that the cuboidal precipitates with grey contrast, highlighted with red arrows in Fig. 1B and C are rich in yttrium and nitrogen, confirming the results from XRD. The average size for Ni grains (Fig. 1E) and large YN inclusions, calculated using the area method from multiple TEM micrographs similar to Fig. 1B, were 262 nm and 185 nm, respectively. In addition to the large YN inclusions, small yttrium nano-dispersoids (highlighted with yellow arrows in Fig. 1C and D and composition shown in Fig. S1E) with an average size of approximately 7 nm (Fig. 1F) were observed to be distributed throughout the material and pinning the grain boundaries (Fig. 1C). The number densities of the large YN inclusions and yttrium nano-dispersoids calculated from TEM micrographs (assuming lamella thickness of 70 nm for both), were on the orders of 10^{19}/ m^3 and $10^{22}/m^3$, respectively. The presence of these yttrium

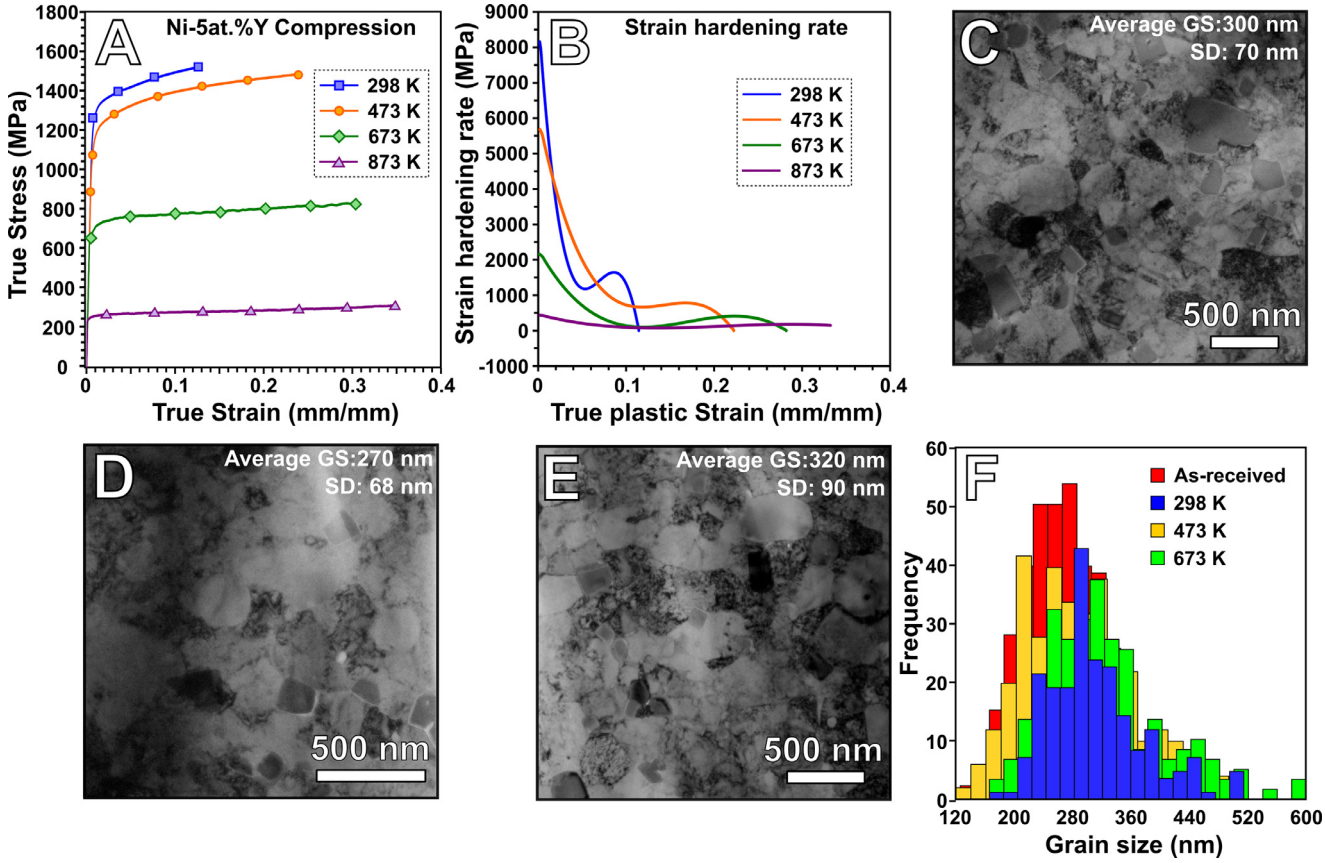

Fig. 2. (A) Compression true stress - true strain response for Ni-Y tested under quasi static strain rate (10^{-4} s^{-1}) at different temperatures. (B) Strain hardening rate under quasi static compression at different temperatures. (C-E) BF TEM images for Ni-Y samples tested at (C) 298 K, (D) 473 K and (E) 673 K. (F) Grain size distribution for Ni grains under multiple post- deformed conditions.

nano-dispersoids with an average spacing of around 25 nm (calculated from TEM images), could play an important role on imparting thermomechanical stability to the microstructure.

To evaluate such thermomechanical behavior, quasi-static compression tests were performed at different temperatures. Fig. 2A represents true stress–true strain data obtained from these tests, which shows that the Ni-Y alloy exhibits an exceptional room temperature yield strength (measured at 0.2% strain) of ~1255 MPa. This room temperature yield strength was retained up to a temperature of 473 K. However, a sharp reduction in strength was observed as the testing temperature was increased beyond 473 K. Additionally, there is a significant strain hardening observed in low temperature tests (298 and 473 K), which gradually disappears at high testing temperatures (673 and 873 K) as seen in Fig. 2B. Fig. 2(C–E) are the post-deformed micrographs of samples compression-tested at 298 K, 473 K, and 673 K. After thermo-mechanical loading, the average grain size at 673 K (~ 0.4 T_m) was around 320 nm, indicating a marginal grain size increase of 25% at a homologous temperature of ~ 0.4 T_m compared to the as-received condition. A comparison of grain size distributions between the compression-tested samples and the as-received material shown in Fig. 2F illustrates that there is a negligible coarsening or shift in the size distribution of the Ni grains, and the alloy maintains its UFG microstructure under significant thermomechanical loading. Post-deformed characterization clearly indicates a negligible increase in the grain size and particle size for the Ni and YN phases, respectively, with the application of thermomechanical loading.

To further examine the thermomechanical response of the alloy under severe conditions such as creep deformation, compression creep experiments were performed at 673 K, which is nearly 40% of the absolute melting temperature for pure Ni (0.4 T_m). Creep experiments were conducted at two different stress levels (constant loading), 30% and 50% of the yield stress at 673 K respectively, for at least 300 h (~ 2 weeks). Fig. 3A represents the creep response for the Ni-Y alloy at 673 K and two different applied stresses. At both levels of applied stresses, i.e. 30% and 50% of the yield stress at 673 K, the steady state creep rate shown by the alloy is on the order of 10^{-8} s^{-1}. This creep rate possessed by the UFG material is comparable to that of Ni based superalloys [23]. TEM characterization of the crept samples (Fig. 3B and C), showed that the average grain size was approximately 350 nm, indicating marginal coarsening as compared to the as-received grain size. This stable behavior is attributed to the kinetic pinning [24,25] offered by the yttrium nano-dispersoids. Furthermore, interaction of dislocations with yttrium nano-dispersoids can be clearly observed in Fig. 3(B–E), which is crucial for enhanced properties, and indicates that dislocation-dispersoid interactions are a creep strengthening mechanism in Ni-Y. These interactions are mainly governed by the coherency of such dispersoids, which tend to be predominantly semi coherent/incoherent at such size range of 7 nm [26].

Next, we evaluate the contribution of different microstructural features on the observed mechanical properties of this alloy. For instance, the ultrafine grain structure with dispersoids could result in Hall–Petch type strengthening as well as the Orowan-type strengthening mechanism. Hence, we performed a theoretical analysis [27] to evaluate such contributions as a function of the temperature, which is discussed below. In case of Ni-Y, the observed flow stress (σ_{flow}) at different temperatures can be represented

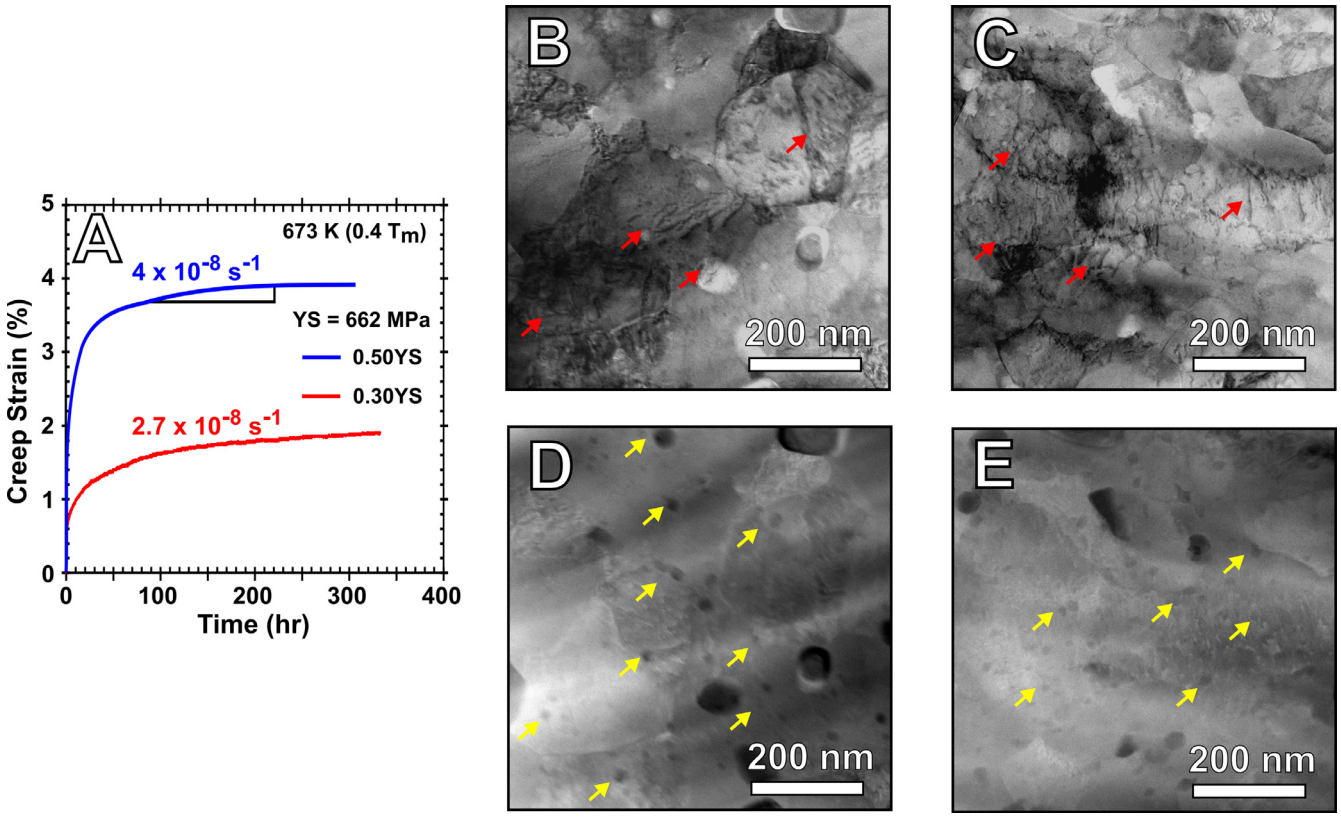

Fig. 3. (A) Compression creep response at 673 K and at 30% and 50% of the yield stress. (B) Post-deformed BF STEM image of the sample tested at 673 K and 30% of the yield stress. (C) Post-deformed BF STEM image of the sample tested at 673 K and 50% of the yield stress. Dislocations are highlighted with red arrows. (D) and (E) are the corresponding HAADF images to (B) and (C) respectively highlighting the nanodispersoids with yellow arrows. (For interpretation of the references to color in this figure legend, the reader is referred to the web version of this article.)

Table 1
The various strengthening mechanisms in Ni-Y operating under uniaxial compression loading. The experimental flow values are taken at 10% strain for curves obtained from uniaxial compression tests at a strain rate of 10^{-4} s^{-1}. The grain size distribution for all the conditions were almost similar within their standard deviations.

σ_{flow} (MPa) Expt	T (K)	d (nm) Expt	σ_{gb} (MPa) H-P prediction	σ_o (MPa) Frictional stress	σ_{or}(MPa) Experiments
1507	298	300	630	22	855
1406	473	270	629	22	755
780	673	320	574	22	184

with the following equation, $\sigma_{flow} = \sigma_o + \sigma_{gb} + \sigma_{or}$, where σ_o is the frictional stress in pure Ni, σ_{gb} is the grain boundary strengthening, and σ_{or} is the Orowan-type strengthening. The frictional stress (σ_o) for pure Ni [28] has a value of 22 MPa and is constant at all temperatures. The strength resulting from grain boundaries, σ_{gb}, at room temperature is governed by the Hall-Petch equation as described in Darling et al. [20] for Ni and Ni-Y systems. However, a shear moduli correction ($\frac{G(T)}{G_o}$) must be applied to their equation in order to determine σ_{gb} at higher temperatures, where G_o and $G(T)$ are the shear moduli at 298 K and at the desired temperature, respectively [28], see supplemental Table S1. The flow stress (σ_{flow}) equation can be rearranged to obtain the residual strength that is associated with thermal activation of dislocation and grain boundary interactions with inclusions/dispersoids at different temperatures, which is listed in Table 1 below.

From the Table 1, $\boldsymbol{\sigma_{or}}$ is 855 MPa and 755 MPa at 298 K and 473 K, respectively, indicating that the Orowan-type strengthening offered by the nano-dispersoids governs the majority of the strength in the Ni-Y alloy. This behavior can be further explained through the general equation of Orowan strengthening ($\frac{Gb}{2\pi\lambda\sqrt{1-\nu}} ln(\frac{d}{r_0})$), where G and ν are the shear modulus and Poisson ratio respectively, b is the Burger's vector of Ni, d is the dispersoid size, r_0 is the outer cut-off radius for matrix dislocations and λ is the dispersoid spacing [29]. The σ_{or} at room temperature of 855 MPa (Table 1) gives a spacing of about ~19 nm based on the Orowan equation, which agrees with the spacing calculated from the TEM micrographs shown in Fig. 1. Additionally, σ_{or}, which is governed by the interaction of dislocations with the nano-dispersoids, is also dependent on the activation energy for looping/bypass. At lower temperatures, activation energy for looping/cutting is generally higher and as the temperature increases the dislocation motion becomes easier due to increase in the thermal contribution for the looping or bypass [30–32]. Thus, the Orowan strength sharply decreases and falls to about 184 MPa beyond 473 K. In other words, engineered nano-dispersoids in Ni-Y alloy are not as effective as nano-clusters in NC Cu-Ta alloys [2], since the latter is able to maintain relative high strength at very high homologous temperatures. Nevertheless, the initial creep characterization for this alloy shows promising results in terms of steady state creep rate and microstructure stability akin to NC Cu-Ta [2] and NC Fe-Zr systems [7]. However, further compositional optimization (including exploring other alloying elements) is needed to improve strength at high homologous temperature. For instance, addition of additional alloy elements could lead to

a stable duplex system [33], thus maintaining strength at relatively high homologous operating temperatures. Development of such behavior is crucial because of (a) high modulus and strength of Ni as compared to other structural FCC metals such as Al, and (b) broader applicability of Ni-based alloy for resilient energy generation and transportation applications. In addition, thermal barrier coatings for Ni-based superalloys can be directly applied to expedite the transition of these alloys to actual systems.

In summary, UFG Ni-Y shows considerable microstructural stability under thermo-mechanical loading up to a homologous temperature of 0.5 T_m. Addition of Y as an alloying element and utilization of non-equilibrium processing techniques demonstrated the contribution of kinetic pinning in retarding rapid grain coarsening under the application of temperature and mechanical loads. Compression creep results for this alloy yielded exceptional creep rates comparable to advanced Ni-based single crystal superalloys. Additionally, uniaxial compression tests were also performed at various temperatures since establishing a relationship between quasi-static and creep properties of the alloy is crucial for its applicability in high temperature structural components. Overall, this study demonstrates that the phenomena of kinetic pinning by appropriate alloying additions can be utilized to achieve tailor-made microstructure for specific applications.

Declaration of Competing Interest

The authors declare that they have no known competing financial interests or personal relationships that could have appeared to influence the work reported in this paper.

Acknowledgments

S.S., C.K., and K. N. S. acknowledge the use of facilities within the LeRoy Eyring Center for Solid State Science at Arizona State University. This work was supported by the US Army Research Laboratory under contract W911NF-15-2-0038 and the National Science Foundation under grants nos. 1663287 and 1810431.

Supplementary materials

Supplementary material associated with this article can be found, in the online version, at doi:10.1016/j.scriptamat.2020.06.068.

References

[1] A. Guinier, Nature 142 (1938) 569–570.
[2] K.A. Darling, M. Rajagopalan, M. Komarasamy, M.A. Bhatia, B.C. Hornbuckle, R.S. Mishra, K.N. Solanki, Nature 537 (2016) 378–381.
[3] K.A. Darling, M.A. Tschopp, R.K. Guduru, W.H. Yin, Q. Wei, L.J. Kecskes, Acta Mater. 76 (2014) 168–185.
[4] M. Rajagopalan, K. Darling, S. Turnage, R. Koju, B. Hornbuckle, Y. Mishin, K. Solanki, Mater. Des. 113 (2017) 178–185.
[5] S. Turnage, M. Rajagopalan, K. Darling, P. Garg, C. Kale, B. Bazehhour, I. Adlakha, B. Hornbuckle, C. Williams, P. Peralta, Nat. Commun. 9 (2018) 2699.
[6] B.C. Hornbuckle, C. Kale, S. Srinivasan, T.L. Luckenbaugh, K.N. Solanki, K.A. Darling, Scr. Mater. 160 (2019) 33–38.
[7] G.B. Shan, Y.Z. Chen, Y.J. Li, C.Y. Zhang, H. Dong, Y.B. Cong, W.X. Zhang, L.K. Huang, T. Suo, F. Liu, Scr. Mater. 179 (2020) 1–5.
[8] B.C. Hornbuckle, T. Rojhirunsakool, M. Rajagopalan, T. Alam, G.P.P. Pun, R. Banerjee, K.N. Solanki, Y. Mishin, L.J. Kecskes, K.A. Darling, JOM 67 (2015) 2802–2809.
[9] M. Rajagopalan, K.A. Darling, C. Kale, S.A. Turnage, R.K. Koju, B.C. Hornbuckle, Y. Mishin, K.N. Solanki, Mater. Today 31 (2019) 10–20.
[10] B.C. Hornbuckle, C.L. Williams, S.W. Dean, X. Zhou, C. Kale, S.A. Turnage, J.D. Clayton, G.B. Thompson, A.K. Giri, K.N. Solanki, K.A. Darling, Commun. Mater. 1 (2020) 1–6.
[11] B.C. Hornbuckle, S.W. Dean, X. Zhou, A.K. Giri, C.L. Williams, K.N. Solanki, G.B. Thompson, K.A. Darling, Appl. Phys. Lett. 116 (2020) 231901.
[12] G.R. Odette, D.T. Hoelzer, JOM 62 (2010) 84–92.
[13] G.R. Odette, Scr. Mater. 143 (2018) 142–148.
[14] C.P. Massey, D.T. Hoelzer, P.D. Edmondson, A. Kini, B. Gault, K.A. Terrani, S.J. Zinkle, Scr. Mater. 170 (2019) 134–139.
[15] T. Ghidini, Nat. Mater. 17 (2018) 846–850.
[16] T.M. Pollock, Nat. Mater. 15 (2016) 809–815.
[17] W.M. Yin, S.H. Whang, R. Mirshams, C.H. Xiao, Mater. Sci. Eng. A 301 (2001) 18–22.
[18] F.A. Mohamed, M. Chauhan, Metall. Mater. Trans. A 37 (2006) 3555–3567.
[19] R.S. Kottada, A.H. Chokshi, Scr. Mater. 53 (2005) 887–892.
[20] K.A. Darling, L.J. Kecskes, M. Atwater, J. Semones, R.O. Scattergood, C.C. Koch, J. Mater. Res. 28 (2013) 1813–1819.
[21] P.S. Singh, Z. Liang, G.M. Pharr, M.P. de Boer, Mater. Sci. Eng. A 784 (2020) 139309.
[22] K. Oh-Ishi, Z. Horita, M. Nemoto, M. Furukawa, T.G. Langdon, Metall. Mater. Trans. A 29 (1998) 2011–2013.
[23] T.M. Pollock, S. Tin, J. Propuls. Power 22 (2006) 361–374.
[24] P. Manohar, M. Ferry, T. Chandra, ISIJ Int. 38 (1998) 913–924.
[25] R.K. Koju, K.A. Darling, K.N. Solanki, Y. Mishin, Acta Mater. 148 (2018) 311–319.
[26] J.D. Eshelby, Proc. R. Soc. Lond. Math. Phys. Eng. Sci. 241 (1957) 376–396.
[27] C. Kale, S. Turnage, P. Garg, I. Adlakha, S. Srinivasan, B.C. Hornbuckle, K. Darling, K.N. Solanki, Mater. Des. 163 (2019) 107551.
[28] J.H. Schneibel, M. Heilmaier, Mater. Trans. 55 (2014) 44–51.
[29] J.F. Nie, B.C. Muddle, I.J. Polmear, Mater. Sci. Forum 217–222 (1996) 1257–1262.
[30] G.E. Dieter, D. Bacon, Mechanical Metallurgy, McGraw-Hill New York, 1986.
[31] J. Hirth, J. Lothe, in: Theory of Dislocations, McGraw-Hill, New York, 1968, p. 780.
[32] I. Adlakha, P. Garg, K.N. Solanki, J. Alloy. Compd. 797 (2019) 325–333.
[33] H.A. Murdoch, C.A. Schuh, J. Mater. Res. 28 (2013) 2154–2163.